# Dynamic Photonic Structures: Stopping, Storage, and Time Reversal of Light

*By Mehmet F. Yanik and Shanhui Fan*

The use of dynamic photonic structures opens fascinating new possibilities for controlling the properties of light. The general idea is to create a coupled resonator array such that a light pulse can be held in the structure for a sufficiently long time, and to modulate the refractive index of the system while the pulse is in the system. Doing so allows the spectrum of the pulse to be molded almost arbitrarily with small refractive index modulations, leading to highly nontrivial information-processing capabilities on chip. As examples of such capabilities, here we show that light pulses can be stopped, stored, and time-reversed with these dynamic systems.

## 1. Introduction

The developments of photonic nanostructures, including photonic crystals [1] and optical microcavities [2], have generated great interest recently. These structures can create optical resonances that confine light within a small modal volume for a relatively long photon lifetime. The strong localization of light has led to very important new applications in quantum and nonlinear optics, such as zero-threshold lasers [3, 4] and low-power optical switches [5–8] and memory elements [9].

Address for correspondence: Shanhui Fan, Ginzton Laboratory, Stanford University, Stanford, CA 94305; e-mail: shanhui@stanford.edu

*STUDIES IN APPLIED MATHEMATICS* 115:233–253


Published by Blackwell Publishing, 350 Main Street, Malden, MA 02148, USA, and 9600 Garsington Road, Oxford, OX4 2DQ, UK.

In this paper, we point out the fascinating new possibilities when dynamic behaviors are introduced into the microresonator systems. By creating a coupled resonator array, a light pulse can be held in photonic structures for sufficiently long times. When a pulse is in such a system, the spectrum of the pulse can be molded almost arbitrarily with a small refractive index modulation, leading to highly nontrivial information-processing capabilities on chip. As examples of such capabilities, here we show that the bandwidth of a light pulse can be compressed to zero, resulting in all-optical stopping and storage of light. We also demonstrate that the spectrum of a light pulse can be inverted to give a time-reversal operation.

A fundamental difficulty in integrated optics has been that different optical functionalities tend to require different material systems. For example, the traditional way to accomplish time reversal through phase-conjugation requires nonlinear optical materials such as $LiNbO_3$ [10]. And light stopping has been demonstrated only in atomic gases under extreme conditions [11, 12]. On the other hand, small refractive index modulations can be readily incorporated into photonic crystal or microresonator systems to create dynamic photonic structures. Thus, the use of dynamic photonic structures, as we envision here, may provide a unifying platform for diverse optical information-processing tasks in the future.

## 2. Tuning photon spectrum

Here we provide a simple example to show how the spectrum of electromagnetic wave can be modified by tuning a structure while the wave is confined in the structure. Consider a linearly polarized electromagnetic wave in one dimension, the wave equation for the electric field can be written as

$$\frac{\partial^2 E}{\partial x^2} - (\varepsilon_0 + \varepsilon(t))\mu_0 \frac{\partial^2 E}{\partial t^2} = 0. \tag{1}$$

Here, $\varepsilon(t)$ represents the modulation and $\varepsilon_0$ is the background dielectric constant. We assume the index modulation $\varepsilon(t)$ to be translationally invariant. Hence, different wavevector components do not mix in the modulation. For one such wavevector component at $k_0$, with electric field described by $E(t) = f(t)e^{i(k_0 x - \omega_0 t)}$, where $\omega_0 = k_0/\sqrt{\mu_0 \varepsilon_0}$, we have

$$-k_0^2 f - [\varepsilon_0 + \varepsilon(t)]\mu_0 \left[ \frac{\partial^2 f}{\partial t^2} - 2i\omega_0 \frac{\partial f}{\partial t} - \omega_0^2 f \right] = 0. \tag{2}$$

With a slowly varying envelope approximation, i.e., by ignoring the $\frac{\partial^2 f}{\partial t^2}$ term, and by further assuming that the index modulations are weak, that is, $e(t) = e_0$,

Equation (2) can be simplified as

$$-i\frac{\partial f}{\partial t} = \frac{\varepsilon(t)\omega_0}{2[\varepsilon(t)+\varepsilon_0]} f \approx \frac{\varepsilon(t)\omega_0}{2\varepsilon_0} f, \tag{3}$$

which has an exact analytic solution

$$f(t) = f(t_0)\exp\left[i\omega_0 \int_{t_0}^{t} \frac{\varepsilon(t')}{2\varepsilon_0} dt'\right], \tag{4}$$

where $t_0$ is the starting time of the modulation. Thus the "instantaneous frequency" of the electric field for this wavevector component is

$$\omega(t) = \omega_0\left(1 - \frac{\varepsilon(t)}{2\varepsilon_0}\right). \tag{5}$$

We note that frequency change is proportional to the magnitude of the refractive index shift alone. Thus, the process defined here differs in a fundamental way from traditional frequency-conversion processes such as sum or difference frequency generation. In a sum or frequency-conversion process, to convert the frequency of light from $\omega_1$ to $\omega_2$, modulations at a frequency $\omega_2 - \omega_1$ needs to be provided. In contrast, in the process described here, regardless of how slow the modulation is, as long as light is in the system, the frequency shift can always be accomplished.

The existence of the frequency shift in dynamic photonic crystal structures has been first pointed out by Reed et al. in their studies of photonic crystals in the presence of shock waves [13, 14]. The shock waves, effectively speaking, induce a large refractive index shift. In practical optoelectronic or nonlinear optical devices, on the other hand, the accomplishable refractive index shift is generally quite small. Thus, in most practical situations the effect of dynamics is prominent only in structures in which the spectral feature is sensitive to small refractive index modulations. This motivates our consideration of the dynamic resonator structures, and our design on Fano interference schemes, which further enhances the sensitivity of such structures to the index modulations.

The translational invariance of refractive index modulations is also important in the application of dynamic systems. By preserving translational invariance, different wavevector components do not mix with each other. Thus, it is far easier to create reversible processes that maintain all the coherent information encoded in the original pulse while the spectrum of the pulse is changed. Below, we use these considerations to demonstrate two remarkable effects: stopping and time reversal of light [15–18].

## 3. Stopping and storing photons with tunable photonic structures

The ability to drastically slow down the propagation speed of light, and to coherently stop and store optical pulses, holds the key to the ultimate control of light, and has profound implications for optical communications [19] and quantum information processing [20, 21]. To reduce the group velocity of light coherently, there are two major approaches, employing either electronic or optical resonances. Dramatic slowdown or even complete stop of light pulses can be accomplished by converting the optical signal into coherent electronic states [11, 12, 22–29]. The use of electronic states, however, imposes severe constraints on the operating conditions. As a result, only a few very special and delicate electronic resonances available in nature possess all the required properties. All the demonstrated operating bandwidths are far too small to be useful for most purposes. The wavelength ranges where such effects can be observed are also very limited. Furthermore, while promising steps have been taken for room temperature operation in solid-state systems, it still remains a great challenge to implement such schemes on-chip with integrated optoelectronic technologies [28, 29].

Consequently, it is of great interest to pursue the control of light speed using optical resonances in photonic structures including dielectric microcavities [30] and photonic crystals [31–33]. Photonic structures can be defined by lithography and designed to operate at any wavelength range of interest. Ultra-high quality factor cavities have been realized on semiconductor chips [34], and group velocities as low as $10^{-2}c$ for pulse propagation with negligible distortion have been experimentally observed in photonic crystal waveguide band edges [35] or with coupled resonator optical waveguides (CROW) [36–38]. Nevertheless, such structures are fundamentally limited by the delay–bandwidth product constraint [39]—the group delay from an optical resonance is inversely proportional to the bandwidth within which the delay occurs. Therefore, for a given optical pulse with a certain temporal duration and corresponding frequency bandwidth, the minimum group velocity achievable is limited. In a CROW waveguide structure, for example, the minimum group velocity that can be accomplished for pulses at 10 Gbit/s rate with a wavelength of 1.55 $\mu$m is no smaller than $10^{-2}c$. For this reason, up to now, photonic structures could not be used to stop light.

Here we present a set of general criteria to overcome the fundamental limit imposed by the delay–bandwidth product in optics [15–18]. These criteria enable one to generate arbitrarily small group velocities for optical pulses with a given bandwidth, while preserving all the coherent information entirely in the optical domain. These criteria can be achieved in optical resonator systems using only small refractive index modulations performed at moderate speeds, even in the presence of losses [15]. In addition, because the bandwidth constraints occur in almost all physical systems that use resonance-enhancement

effects. The underlying principles are applicable to a wide range of systems and applications.

To coherently stop an optical pulse with a given bandwidth in an all-optical system, the following criteria must be satisfied.

1. The system must possess large tunability in its group velocity. To allow for an optical pulse with a given bandwidth to enter the system, the system must possess an initial state with a sufficiently large bandwidth (i.e., a large group velocity as required by the delay–bandwidth product) to accommodate all the spectral components of the pulse. We design a system such that a small refractive index shift can change the group velocity by many orders of magnitude, and that the group velocity reduction is independent of losses.
2. The tuning of the system needs to be performed in a manner such that the bandwidth of the pulse is reversibly compressed. Such bandwidth compression is necessary to accommodate the pulse as the system bandwidth is reduced. Thus, the tuning process must occur while the pulse is completely in the system, and must be performed in an adiabatic [40] fashion to preserve all the coherent spectral information encoded in the original pulse. The modulation accomplishes a coherent frequency-conversion process for all spectral components, and reversibly compresses the bandwidth of the incident pulse.

To implement the general criterion, we consider a translationally invariant system (Figure 1), in which a waveguide is coupled to two side cavities in each unit cell. The cavities have resonant frequencies $\omega_A$ and $\omega_B$, respectively. This system represents an all-optical analogue of atomic systems exhibiting electromagnetically induced transparency (EIT). Each optical resonance here

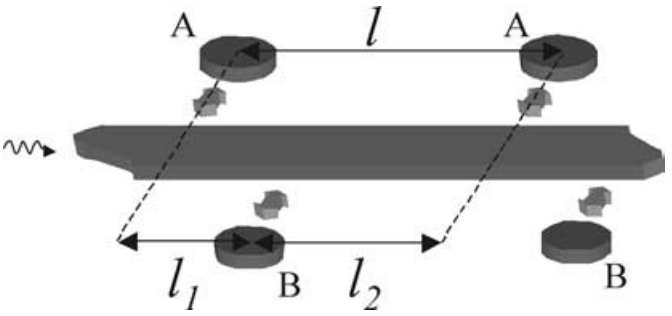


Figure 1. Schematic of a tunable waveguide system used to stop light. The disks and block represent the cavities and the waveguide. The arrows indicate available evanescent coupling pathways between the cavities and the waveguide. The system consists of a periodic array of two side cavities coupled to waveguide, with a coupling rate of $1/\tau$. The distance between the nearest neighbor side cavities is $l_1$, and the length of the unit cell is $l = l_1 + l_2$.

is analogous to the polarization between the energy levels in the EIT system. Initially, we assume that the cavities couple to the waveguide with equal rate of $1/\tau$, and we ignore the direct coupling between the side cavities. The transmission matrix for a waveguide side coupled to a single resonator with resonance frequency $\omega_i$ can be calculated using the Green's function method [41] as

$$T_{c_i} = \begin{pmatrix} 1 + j/(\omega - \omega_i)\tau & j/(\omega - \omega_i)\tau \\ -j/(\omega - \omega_i)\tau & 1 - j/(\omega - \omega_i)\tau \end{pmatrix}. \tag{6}$$

The transmission matrix through an entire unit cell in Figure 1 can then be determined as

$$T = T_{c_1} T_{l_1} T_{c_2} T_{l_2}, \tag{7}$$

where

$$T_{l_i} = \begin{pmatrix} e^{-j\beta l_i} & 0 \\ 0 & e^{j\beta l_i} \end{pmatrix}$$

is the transmission matrix for a waveguide section of length $l_i$. Here, $\beta$ is the wavevector of the waveguide at a given frequency $\omega$.

Because $\det(T) = 1$, the eigenvalues of $T$ can be represented as $e^{ikl}, e^{-ikl}$, where $l = l_1 + l_2$ is the length of the unit cell, and $k$ (when it is real) corresponds to the Bloch wavevector of the entire system. Therefore, we obtain the band diagram of the system as

$$\frac{1}{2}\mathrm{Tr}(T) = \cos(kl) = f(\omega) \equiv \cos(\beta l) + \frac{C_+}{(\omega - \omega_\mathrm{A})} + \frac{C_-}{(\omega - \omega_\mathrm{B})}, \tag{8}$$

where

$$C_\pm = \frac{2\sin(\beta l_1)\sin(\beta l_2)}{(\omega_\mathrm{A} - \omega_\mathrm{B})\tau^2} \pm \frac{\sin(\beta l)}{\tau}.$$

In the frequency range where $|f(\omega)| < 1$, the system supports propagating modes, while $|f(\omega)| > 1$ corresponds to the frequency ranges of the photonic band gaps. For a large frequency separation $\Delta = |\omega_\mathrm{A} - \omega_\mathrm{B}|\tau$, the band diagram is shown in Figure 2a. In the vicinity of the resonances, the system supports three photonic bands, with two gaps occurring around $\omega_\mathrm{A}$ and $\omega_\mathrm{B}$. Such a band diagram is similar to that of EIT systems [42].

The width of the middle band depends strongly on the resonant frequencies $\omega_\mathrm{A}$, $\omega_\mathrm{B}$. Importantly, when the resonant frequencies satisfy the following

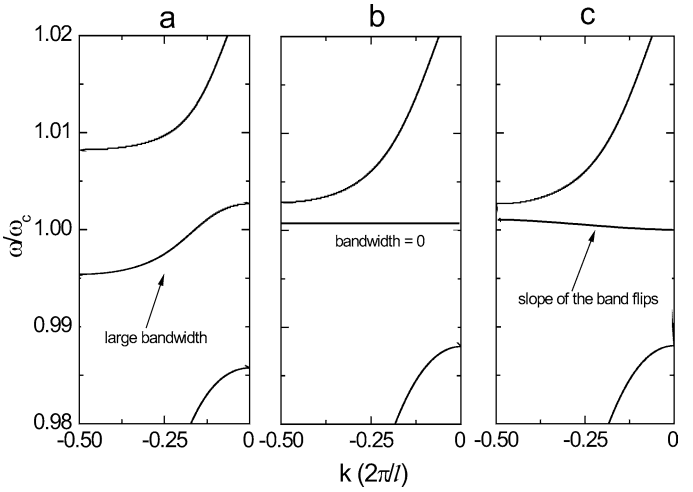


Figure 2. The photonic bands of the system of Figure 1 for three different choices of $\Delta \equiv |\omega_A - \omega_B|\tau$. (a) $\Delta = 3.277$, the bandwidth of the middle band is large. (b) $\Delta \approx 0.341$, the bandwidth goes to zero. (c) $\Delta = 0$, the slope of the band flips its sign. The cavity resonance frequencies are given by $\omega_{A,B} = w_c \pm \Delta/2\tau$, where $\omega_c = 0.357(2\pi c/a)$ and $1/\tau = \omega_c/235.8$. Here, $a$ is a length unit. The distances between the cavities are $\ell_1 = 2a$ and $\ell = 8a$. The waveguide has a dispersion of $\beta = [0.278 + 0.327(\omega a/2\pi c - 2.382)]/a$, which is actually a fit for the photonic crystal waveguide in Figure 3.

conditions, the width of the middle band becomes zero (Figure 2b), with the frequency of the entire band pinned at $\omega_A$:

$$C_+(\omega_A) = \frac{2\sin[\beta(\omega_A)l_1]\sin[\beta(\omega_A)l_2]}{(\omega_A - \omega_B)\tau^2} + \frac{\sin[\beta(\omega_A)l]}{\tau} \to 0 \qquad (9)$$

$$\left|\cos[\beta(\omega_A)l] + \frac{C_-(\omega_A)}{\omega_A - \omega_B}\right| > 1. \qquad (10)$$

(Alternatively, the band can be pinned at $\omega_B$ with a similar condition.) To prove these conditions, we note that $f(\omega)$ in Equation (8) has a singularity at $\omega = \omega_A$. The frequency width of this singularity is controlled by $C_+(\omega_A)$, and approaches zero when Equation (9) is satisfied. Satisfying Equation (10), on the other hand, ensures that the solutions to $|f(\omega)| \leq 1$ in the vicinity of $\omega_A$ occurs on the same branch of the singularity $1/(\omega - \omega_A)$, and thus forms a continuous band. When both conditions are satisfied, as the width of the singularity approaches zero, a band (the middle band in Figure 2b) always exists in the vicinity of $\omega_A$, and the width of this middle band vanishes. Upon further decrease of $\Delta$, the group velocity of the band changes sign (Figure 2c).

Furthermore, the sign of the group velocity for the middle band can be designed by choosing appropriate $l_1$ and $l_2$.

In the presence of direct coupling due to photon tunneling between the two cavities in the same unit cell, one could still describe the system in terms of two resonant eigenstates within each unit cell. The dispersion can be expressed in the same functional form as of Equation (8) with $\omega_A$ and $\omega_B$ in the denominator replaced by the frequencies of the eigenstates. And bandwidth compression to zero still occurs when $\Delta$ satisfies conditions analogous to that of Equations (9) and (10). This is also supported by our numerical observations that the sign of the band flips. In addition, in photonic crystals, the direct coupling constant decreases exponentially with the distance between the cavities, and can, therefore, be reduced to any desired value in our system because the cavities are not across each other along the waveguide. Our simulations also indicate that even in the presence of loss, extremely flat band is obtainable, and the sign of the band still flips, which is consistent with our previous finding in a different system [15]. In general, it appears that the group velocity becomes independent of the loss when the losses of different subsystems are matched [15, 18]. In this case, the storage time is limited only by photon lifetime and can be rather long.

The system presented above satisfies the general criterion required to stop light [15]: the system is translationally invariant, and the width of one of the bands can be reversibly compressed to zero. Thus, the dynamic process in [15] can also be applied here to stop a light pulse. We start with large $\Delta$, such that the middle band has a large bandwidth, and $\omega_A$, $\omega_B$ are chosen such that this band can accommodate the incoming pulse, with each spectral component of the pulse occupying a unique wavevector (Figure 2a). After the pulse is completely in the system, we vary $\omega_A$ and $\omega_B$ until the bandwidth of the band is reduced to zero (Figure 2b), at a rate slow compared with the frequency separation of the middle band from other bands.

The system presented above can be implemented in a photonic crystal of a square lattice of dielectric rods ($n = 3.5$) with a radius of $0.2a$, ($a$ is the lattice constant) embedded in air ($n = 1$) (Figure 3) [15]. The photonic crystal possesses a band gap for TM modes with electric field parallel to the rod axis. A single-mode waveguide is generated by removing one row of rods along the pulse propagation direction. Decreasing the radius of a rod to $0.1a$ and the dielectric constant to $n = 2.24$ generates a single-mode cavity with resonance frequency at $\omega_c = 0.357(2\pi c/a)$. The nearest neighbor cavities are separated by a distance of $\ell_1 = 2a$ along the propagation direction, and the unit cell periodicity is $\ell = 8a$. The waveguide–cavity coupling occurs through barrier of one rod, with a coupling rate of $1/\tau = \omega_c/235.8$. The resonant frequencies of the cavities are tuned by refractive index modulation of the cavity rods.

We simulate the entire process of stopping light for $N = 100$ pairs of cavities with finite-difference time-domain (FDTD) method [43], which solves

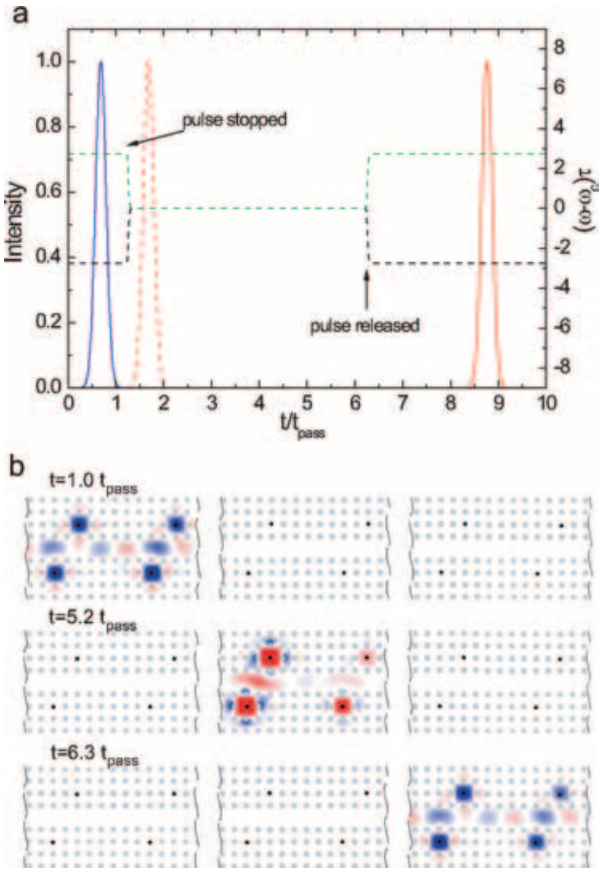


Figure 3. Propagation of an optical pulse through a waveguide–resonator complex in a photonic crystal system as the resonant frequencies of the cavities are varied. The photonic crystal consists of 100 cavity pairs. Fragments of the photonic crystal are shown in part (b). The three fragments correspond to unit cells 12–13, 55–56, 97–98. The dots indicate the positions of the dielectric rods. The black dots represent the cavities. (a) The dashed green and black lines represent the variation of $\omega_A$ and $\omega_B$ as a function of time, respectively. The blue solid line is the intensity of the incident pulse as recorded at the beginning of the waveguide. The red dashed and solid lines represent the intensity at the end of the waveguide, in the absence and the presence of modulation, respectively. (b) Snapshots of the electric field distributions in the photonic crystal at the indicated times. Red and blue represent large positive and negative electric fields, respectively. The same color scale is used for all the panels.

Maxwell's equations without approximation. The computational cell is truncated by uniaxial perfectly matched boundary layers (UPML) [43]. Furthermore, we have used a large enough computational cell such that the result is free of any parasitic reflection from the right end of the computational boundary. The dynamic process for stopping light is shown in Figure 3a. We generate a Gaussian pulse in the waveguide. (The process is independent of the pulse

shape.) The excitation reaches its peak at $t = 0.8t_{\text{pass}}$, where $t_{\text{pass}}$ is the traversal time of the pulse through the unmodulated waveguide. During the pulse generation, the cavities have a large frequency separation. The field is concentrated in both the waveguide and the cavities (Figure 3b, $t = 1.0t_{\text{pass}}$), and the pulse propagates at a high speed of $v_g = 0.082c$. After the pulse is generated, we gradually reduce the frequency separation $\Delta$ to zero. During this process, the speed of light is first reduced to zero, and then changes its sign and the pulse starts propagating backward slowly. (The sequence of the corresponding band structure is shown in Figure 2.) As the bandwidth of the pulse is reduced, the field concentrates in the cavities (Figure 3b, $t = 5.2t_{\text{pass}}$). We use an index modulation with a form of $\exp[-t^2/\tau_{\text{mod}}^2]$, where $\tau_{\text{mod}} = 5\tau$. However, almost any modulation pattern and rate would satisfy adiabaticity in this system, as long as the instantaneous rate is small enough compared with the frequency separation between the bands at that particular instance. When zero group velocity is reached, the photon pulse can be kept in the system as a stationary waveform for any time duration. In this simulation, we store the pulse for a time delay of $5.0t_{\text{pass}}$, and then release the pulse by repeating the same index modulation in reverse (Figure 3b, $t = 6.3t_{\text{pass}}$). The pulse intensity as a function of time at the right end of the waveguide is plotted in Figure 3a, and shows the same temporal shape as both the pulse that propagate through the unmodulated system, and the initial pulse recorded at the left end of the waveguide. Thus, the pulse is perfectly recovered without distortion after the intended delay. In the FDTD simulations, we choose an index modulation of 1% and a modulation rate of 1.1 THz only to make the total simulation time feasible. The use of such extremely fast modulation demonstrates that adiabaticity requirement in this system can be achieved easily. The simulation demonstrates a group velocity reduction to zero for a 4-ps pulse at 1.55 $\mu$m wavelength.

This system represents an optimal implementation of the general criterion for stopping light.

1. Only two resonators per unit cell are needed for the bandwidth to be compressed to absolute zero.
2. The same system can be used for time reversal. The slope of the band can change sign as one modulates the resonant frequencies, which results in a time-reversal operation on the pulse [16].
3. This system can operate with fast modulation rates while maintaining adiabaticity, which enables the use of the shortest waveguide. The total length of the waveguide $L$ is determined by the initial bandwidth of the pulse, which sets the maximum speed in the waveguide $v_{g0}$, and by the duration of the modulation $\tau_{\text{mod}}$, which sets the distance that the pulse travels before it is stopped (i.e., $L \sim v_{g0}\tau_{\text{pulse}} + v_{g0}\tau_{\text{mod}}$, where $\tau_{\text{pulse}}$ is the length of the pulse). Due to the delay–bandwidth product, $v_{g0}\tau_{\text{pulse}}$

is a constant independent of the signal bandwidth $\delta\omega$, and the length of the system can thus be estimated as $L \sim (10 + \delta\omega\tau_{\text{mod}})l$ . In this system, the gaps surrounding the middle band have sizes of the order of the cavity–waveguide coupling rate $1/\tau$, and are approximately independent of the slope of the middle band (Figure 2). Thus, by *increasing* the waveguide-coupling rate of the cavity, this gap can be made large, which enables the use of fast modulation while satisfying adiabaticity [15] and significantly reduces the length requirement of the structure. To accomplish the entire process of stopping and recovering a 100-ps pulse, for example, a waveguide with a length less than 30 microcavities modulated at a maximum speed of 20 GHz is sufficient.

4. This system can compress the largest possible pulse bandwidth for a given refractive index modulation strength $\delta n$ . For a resonance with frequency $\omega$, the largest frequency shift possible for a given index modulation is about $\omega\delta n/n$. Therefore, the largest compressible system bandwidth is approximately [15]

$$\delta\omega \simeq \omega\delta n/n, \tag{11}$$

which sets the largest bandwidth of a pulse that can be stopped. The introduced system can achieve this optimal utilization of the system bandwidth. The dispersion over most of the bandwidth is small compared with typical CROW band due to existence of long-range through-waveguide coupling between the cavities. Such reduction in dispersion is particularly prominent when the bandwidth is smaller than $1/\tau$. In the band structure of Figure 2a, because we used large index shifts to make FDTD simulations feasible, the band exhibits large dispersion. In practice, by operating in a regime where $\delta n = 1/\tau\omega_c$, the dispersion over most part of the band is practically negligible. Furthermore, all dispersive effects scale with the second or higher orders of the system bandwidth, while the pulse delay ($\sim 1/v_g$) scales inversely with the system bandwidth. The dispersive effects integrated over time approaches zero in the limit of vanishing bandwidth. In this system, the presence of a zero-width band thus significantly reduces the effects of dispersion, and also results in a more efficient utilization of system bandwidth.

The all-optical EIT-like system represents dramatic improvement over the atomic/electronic schemes for stopping light. For a small refractive index shift of $\delta n/n = 10^{-4}$ achievable in practical optoelectronic devices [44], and assuming a carrier frequency of approximately 200 THz, as used in optical communications, the achievable bandwidths are of the order of 20 GHz, which is comparable to the bandwidth of a single wavelength channel in high-speed optical systems. In comparison, the atomic stop-light schemes have experimentally demonstrated bandwidths less than 100 kHz [11, 12, 28,

29]. The storage times are limited only by the cavity lifetimes. The loss in optical resonator systems might be counteracted with the use of gain media in the cavities [45], or with external amplification. Such capabilities could be important for the use of such schemes in optical communication systems. The loss in principle can also be suppressed with the use of three-dimensional photonic crystals. In such 3D crystals, the loss is only limited by intrinsic material losses. By using high-quality semiconductors or insulators, and by operating at wavelengths below the mid-electronic band gap, the material loss might be quite low, and one might speculate that the lifetime of optical resonators might eventually exceed that of atomic resonances. For example, the material loss lifetime in fused silica is in fact of the order of $10^{-3}$ s, and cavity quality factors ($Q \simeq 8 \times 10^9$) approaching this limit have already been measured in quartz microspheres [46]. Furthermore, optical modes with quality factors approaching $5 \times 10^8$ with large spectral spacing have also been demonstrated in integrated resonators [47]. In addition, materials with losses lower than silica for microresonators are foreseeable. With such long lifetime resonators, optical pulses can be stopped for durations sufficient for quantum information-processing purposes.

## 4. Time reverse of light with tunable photonic structures

The capability to reverse a wave in time has profound scientific and technological implications. Examples of applications include detection through random media, adaptive optics, subwavelength focusing, and dispersion compensation [48–56]. In acoustics or electronics, where the frequencies are low, time reversal can be accomplished by electronic sampling, recording, and playing back [49, 50]. For optical waves, on the other hand, because fields oscillate at higher frequencies, all the mechanisms for time reversal up to now required nonlinear processes such as near-degenerate four-wave mixing [56]. Such nonlinear processes can phase conjugate a monochromatic wave. However, for a pulse, phase matching needs to be satisfied over the entire pulse bandwidth, which presents a challenge to the development of nonlinear materials. In addition, such processes require high-power lasers, which limit on-chip integration.

Here we present a dynamic photonic system that can be used to time reverse optical pulses by only linear optics and electro-optic modulators [16]. No knowledge of the time-dependent phase or amplitude of the light is necessary. Thus, electronic or optical sampling at optical frequencies is not required. Moreover, no nonlinear multiphoton process is required here, which greatly broadens the choices of materials.

Consider a pulse $\psi(t) = A(t, x)e^{i(\omega_c t - k_c x)} + \text{c.c.}$, where $e^{i(\omega_c t - k_c x)}$ is the carrier wave with frequency $\omega_c$ and wavevector $k_c$. $A(t, x)$ is the complex

envelope that carries information. The envelope $A(t, x)$ can be decomposed into its Fourier components as

$$A(t, x) = \sum_k A_k e^{-i(k-k_c)x} e^{i\Delta\omega_k t}. \tag{12}$$

Here $k$ is a wavevector component, and $\Delta\omega(k) = \omega(k) - \omega_c$ is the frequency detuning. The time-reversed pulse envelope $A(-t)$ has a Fourier decomposition of

$$A(-t, x) = \sum_k A_k e^{-i(k-k_c)x} e^{-i\Delta\omega_k t}. \tag{13}$$

Thus, time reversal can be achieved if the frequency of a Fourier component with detuning $\Delta\omega_k$ is converted to a new frequency with detuning $-\Delta\omega_k$, and if such frequency conversion is performed for all Fourier components of the pulse [56]. To preserve wavevector information, such a conversion process should be translationally invariant. Therefore, the pulse should be inside the system during the time-reversal process.

To achieve such frequency conversion, we consider a system consisting of two translationally invariant subsystems A and B (Figure 4). Each subsystem is a CROW structure [36, 37], with nearest-neighbor evanescent coupling rates of $\alpha_A$ and $\alpha_B$, respectively. The subsystems also evanescently couple to each other with a coupling rate of $\beta$. The system is translationally invariant. The dynamics of the field amplitudes $a_i$ and $b_i$ for cavities A and B in the $i$th unit cell can be expressed using coupled mode theory

$$\frac{da_i}{dt} = i\omega_A a_i + i\alpha_A(a_{i-1} + a_{i+1}) + i\beta b_i - \gamma_A a_i \tag{14}$$

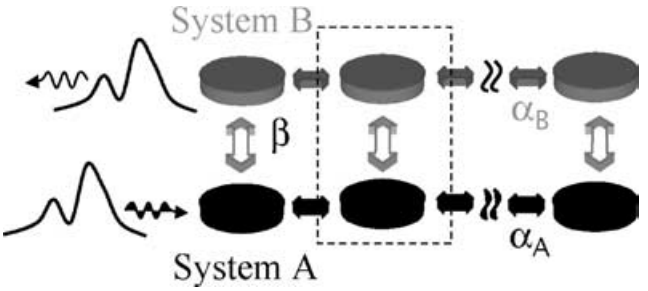


Figure 4. Schematic of a tunable microcavity system used to time reverse light. The disks represent cavities, and the arrows indicate available evanescent coupling pathways between the cavities. The system consists of two subsystems A and B represented by blue and red colors, respectively. Each subsystem A and B consists of a periodic array of coupled cavities. Within each subsystem, the cavities couple to their nearest neighbors with rates $\alpha_A$ and $\alpha_B$, respectively. The two subsystems are also coupled with rate $\beta$.

$$\frac{db_i}{dt} = i\omega_B b_i + i\alpha_B(b_{i-1} + b_{i+1}) + i\beta a_i - \gamma_B b_i. \tag{15}$$

Here $\omega_A$ and $\omega_B$ are the resonance frequencies, and $\gamma_A$ and $\gamma_B$ are the loss rates for the cavities A and B, respectively. For time reversal, we choose $\alpha_A = -\alpha_B \equiv -\alpha$ such that the two CROW waveguides have opposite dispersion relations. The eigenfrequencies $\omega_{\pm,k}$ of the system with a wavevector $k$ can be derived as

$$\omega_{\pm,k} = \frac{1}{2}\left[\omega_{A,k} + \omega_{B,k} + i(\gamma_A + \gamma_B) \pm \sqrt{(\omega_{A,k} - \omega_{B,k} + i(\gamma_A - \gamma_B))^2 + 4\beta^2}\right], \tag{16}$$

where $\omega_{A,k} = \omega_A - 2\alpha\cos(k\ell)$ and $\omega_{B,k} = \omega_B + 2\alpha\cos(k\ell)$ are the frequency bands of the subsystems A and B by themselves, respectively. $\ell$ is the distance between the nearest neighbor cavities in subsystem A or B. The shapes of the bands become independent of losses when $\gamma_A$ and $\gamma_B$ are equal, which can be adjusted externally.

In this system, a pulse can be time reversed by the following process. We start with $\omega_A - \omega_B \ll -|\beta|$, such that the lower band exhibits the characteristic of the subsystem A (Figure 5a). By placing $\omega_A$ at the pulse carrier frequency $\omega_c$ (Figure 5a), the lower band can accommodate the pulse, with each spectral component of the pulse occupying a unique wavevector. After the pulse is in the system, we vary $\omega_A$ and $\omega_B$ until $\omega_A - \omega_B \gg |\beta|$ (Figure 5c), at a rate that is slow compared with the frequency separation between the lower and the upper bands. (The frequency separation reaches minimum $2|\beta|$ when $\omega_A = \omega_B$, Figure 5b.) The modulation of the cavity resonances preserves translational symmetry. Therefore, cross talk between different wavevector components of the pulse is prevented. Also, the slow modulation rate ensures that each wavevector component of the pulse follows only the lower band, with negligible scattering into the upper band (i.e., the system evolves in an adiabatic [40] fashion). Consequently, an initial state with a wavevector $k$ and detuning $\Delta\omega_k$ evolves into a final state with the same wavevector but an opposite detuning of $-\Delta\omega_k$. The spectrum of the incident pulse is thus inverted while the information encoded in the pulse is preserved. Such a spectral inversion process generates a time-reversed version of the original pulse, which moves in subsystem B backward to its original propagation direction, and exits the system. The modulation can follow any adiabatic trajectory in time, and can have a narrower spectrum than the pulse.

Such a system can be implemented in a photonic crystal as shown in Figure 6 [16]. Increasing the radius of one of the high-index rods to $0.5a$ generates a singly degenerate mode at $\omega_0 = 0.286(2\pi c/a)$. We construct two CROW waveguides, each consisting of an array of such cavities (Figure 6). These two CROW waveguides form the subsystems A and B. Coupling between two

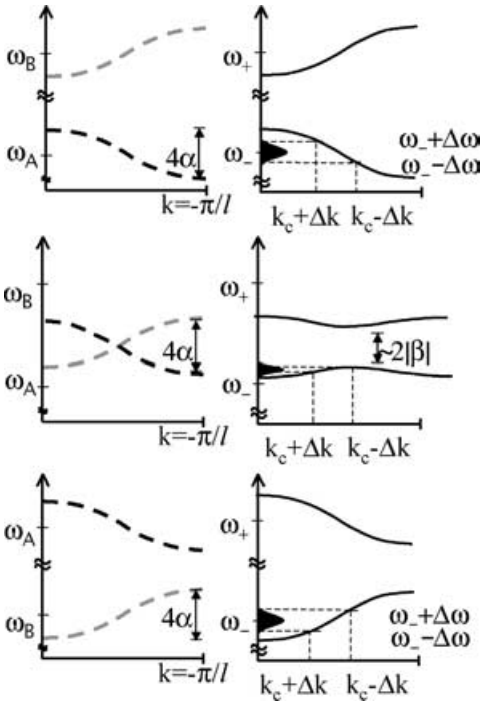


Figure 5. Schematic of the frequency bands for the system shown in Figure 4. $\omega_A$ and $\omega_B$ are the resonance frequencies for individual cavities in subsystems A and B, respectively, and $k$ is the wavevector. In the left panels, the dashed curves correspond to the bands for subsystems A and B, respectively, when the subsystems are not coupled to each other. The cavities in A are coupled to each other via a negative coupling rate, thus the blue curve has a negative group velocity. The cavities in B are coupled to each other via a positive coupling constant, thus the red curve has a positive group velocity. The right panels are the band structures $\omega_+$ and $\omega_-$ of the coupled system. The figure includes three cases: (a) $\omega_A - \omega_B \ll -|\beta|$. The lower frequency band $\omega_-$ exhibits the characteristic of the subsystem A with negative group velocity, and it is centered at the pulse carrier frequency $\omega_c$ to accept an incoming pulse. (b) $\omega_A \approx \omega_B$. The subsystems A and B are near resonant. The upper and lower bands of the system display a mixed character of both subsystems of A and B. Here, the distance between the upper and lower bands is near its minimum $|\omega_+ - \omega_-| \approx 2|\beta|$. (c) $\omega_A - \omega_B \gg |\beta|$. The lower frequency band $\omega_-$ exhibits the characteristic of the subsystem B with positive group velocity.

neighboring cavities of the subsystem A occur through a barrier of five rods ($\ell = 6a$), with a rate of $\alpha_A = -1.89 \times 10^{-3}(2\pi c/a)$. The two subsystems A and B are coupled with a rate of $\beta = -1.89 \times 10^{-3}(2\pi c/a)$. The resonant frequencies of the cavities can be tuned by refractive index modulations of the dielectrics within the cavities. In subsystem B, we introduce air cylinders with radius $0.2a$ in the middle of the barriers. In a CROW waveguide, the band-edge state at $k = 0$ has significant energy in the center of the barriers, while the band-edge state at $k = \pi/\ell$ has a nodal plane at the same location.

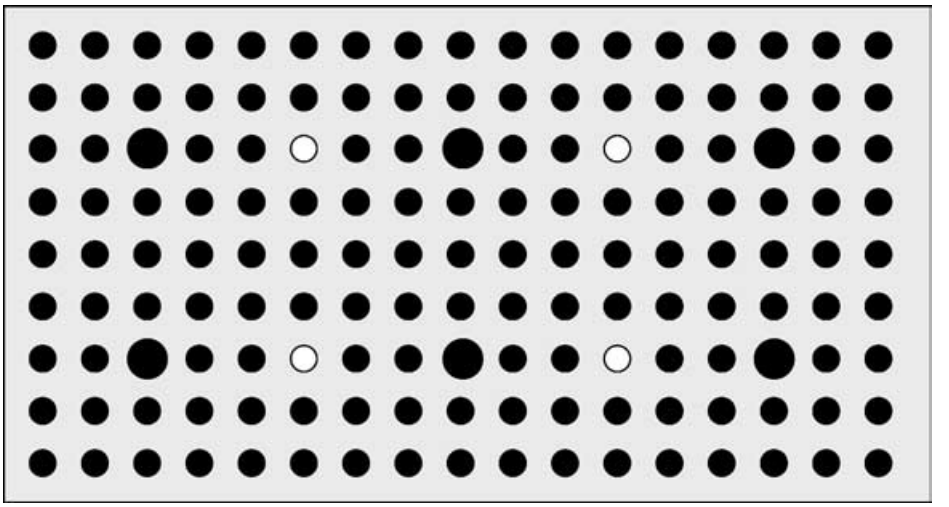

Figure 6. An implementation of the general system of Figure 4 in a two-dimensional photonic crystal. The crystal consists of high index ($n = 3.4$) rods in a low-index material ($n = 1.5$) indicated by the gray background. The small black dots indicate the positions of the dielectric rods. These rods have a radius of $0.2a$, where $a$ is the lattice constant. The large black dots represent dielectric rods with a radius of $0.5a$ and with tunable index near 3.4. These dots form the subsystems A and B. The white holes indicate air cylinders with radius $0.2a$.

Thus, by adjusting the dielectric between the cavities, the dispersion of the CROW waveguide can be strongly affected. Our choice for the radius of the air cylinders yields $\alpha_B = 1.89 \times 10^{-3}(2\pi c/a) = -\alpha_A$.

We simulate a system with 100 pairs of cavities using FDTD method 43. The subsystems are terminated by introducing a loss rate equal to $|\alpha_{A,B}|$ in the last cavities. This provides a perfect absorbing boundary condition. Initially, we generate an asymmetric pulse (Figure 7a) by exciting the first cavity. The excitation has a large peak at $t = 0.5 \cdot t_{pass}$ and a smaller peak at $t = 0.75t_{pass}$, where $t_{pass}$ is the traversal time of the pulse through the system without any index modulation. While the pulse is generated, the subsystem A is in resonance with the pulse frequency, while the subsystem B is kept detuned. The field is concentrated in the subsystem A (Figure 7b, upper panel, $t = 0.8t_{pass}$), and the pulse propagates at a group velocity of $2\alpha_A\ell$. After the pulse is generated, we gradually tune the subsystem B into resonance with the pulse while de-tune the subsystem A out of resonance (Figure 7a, $t = 1.25t_{pass}$). At the end of this process, the field is transferred from the subsystem A to the subsystem B (Figure 7b lower panel, $t = 1.2t_{pass}$). We used a modulation $\exp[-t^2/t_{mod}^2]$ where $t_{mod} = 10/\beta$, which is sufficient to preserve adiabaticity. The pulse at the exit of the subsystem B shows the perfect time-reversed temporal shape of the initial pulse at the entrance of the subsystem A (Figure 7a). In the FDTD

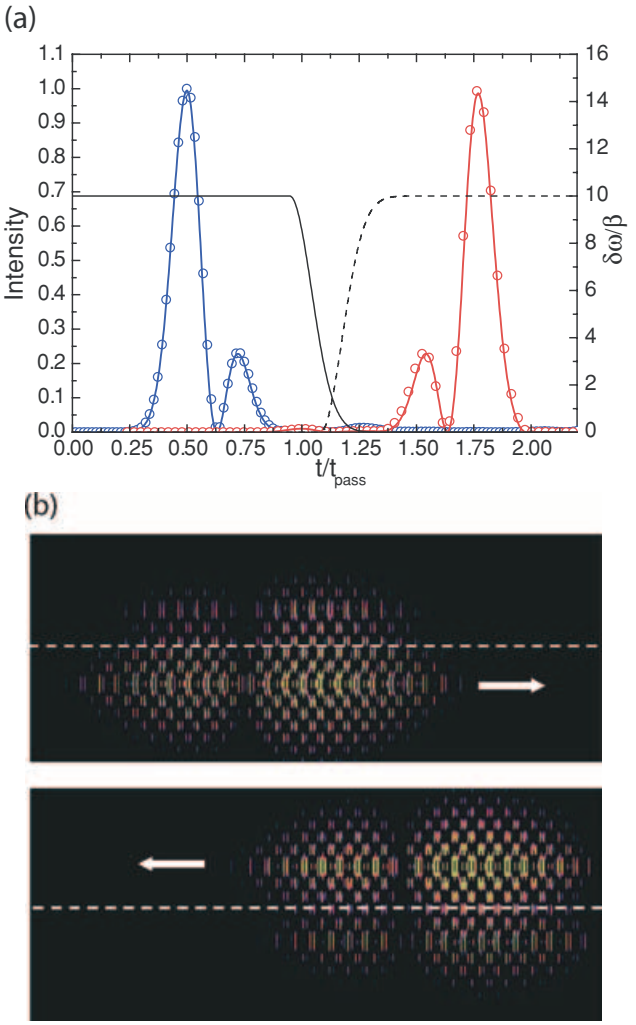


Figure 7. Propagation of an optical pulse through a coupled microcavity complex in a photonic crystal system as the resonance frequencies of the cavities are varied. The photonic crystal consists of 100 cavity pairs. The pulse is generated by exciting the first cavity. (a) The dashed and solid black lines represent the variation of resonance frequencies $(\omega_{A,B} - \omega_c)/\beta \equiv \delta\omega/\beta$ as a function of time, respectively. The blue and the red lines represent the electromagnetic intensity as recorded in the middle of subsystems A and B, respectively. $t_{pass}$ is the traversal time of the pulse through the system when no index modulation is applied. Open circles are FDTD results, and the red and blue lines are from coupled mode theory. (b) Snapshots of the electric field distributions in the photonic crystal at $t = 0.8t_{pass}$ and $t = 1.2t_{pass}$, in the upper and lower panels, respectively. The dimensions of the images along the propagation direction are compressed. Yellow represents large positive electric fields. The same color scale is used for both panels. The arrows indicate propagation direction of the pulse, and the dashed lines represent the locations halfway in between subsystems A and B.

simulations, to make the total simulation time feasible, we choose a large index modulation of about 6% and a modulation rise time of about 10 ps. We have also performed coupled mode theory calculations using Equations (14) and (15), where the effects of index change are taken into account by the modulation of the resonant frequencies, while the coupling constants are kept unchanged. This approach is valid as long as the frequency change is small. The results show excellent agreement with FDTD (Figure 7a).

Coupled mode theory allows us to determine the system requirements in practical optoelectronic devices, because the modulation strengths ($\delta n/n$) are typically less than $10^{-4}$ [44]. The number of cavities is determined by the pulse length and the duration of the time-reversal process. The duration of time reversal can be reduced by using a large $\beta$ because the fastest modulation rate is limited by $\beta$. The largest coupling $\beta$ that can be used is limited by the strength of index modulations. To accommodate a pulse, the coupling constants $|\alpha_{A,B}|$ needs to be larger than the bandwidth of the pulse. In a photonic bandgap, both $|\alpha_{A,B}|$ and $\beta$ decrease exponentially with the distance between the cavities, and also depend on the bandgap size. The coupling constants can, therefore, be designed by choosing appropriate distances and lattice constants in photonic crystals [33]. With a refractive index modulation of the order of $10^{-4}$ at a maximum modulation speed of 100 GHz, about 100 microcavities are sufficient to time reverse an pulse with a 20 GHz bandwidth centered at 200 THz. Independent modulation of only two sets of cavities (i.e., A and B in Figure 4) is required. With electro-optical modulation of high-Q microcavities [57], chip-scale implementation of such systems is foreseeable.

## 5. Conclusion

The on-chip and room temperature operation of dynamic photonic structures may enable completely new classical and quantum information-processing capabilities. Multiple pulses can be held simultaneously in the system, and desired pulses can then be released on demand. This capability might enable controlled entanglement of networks of quantum systems in distant microcavities via photons, thus opening up the possibility of chip-scale photonic quantum information processing. We further note that the technique of coherent field transfer between multiple systems (Figure 5) can be used to combine all-optical systems and atomic systems to overcome some of the fundamental bandwidth and wavelength limitations in the atomic systems. For example, the first few subsystems of such a system can be all-optical resonators with a large bandwidth to accommodate a fast optical pulse, and the last subsystem can consist of nuclear spin states with long lifetimes to store the electromagnetic coherence.

The ultra-low group velocity and bandwidth compression also dramatically enhances nonlinear effects over the entire bandwidths of pulses. Also, the

stopping of light occurs at a single photon level. Thus, the work could have important implications for quantum information processing, especially when the group velocity is ultra low.

The small index modulations that are required can readily be achieved with the intrinsic nonresonant electro-optical effects in semiconductors, without requiring resonant electronic excitations that are intrinsically lossy. Moreover, fluctuations in microcavity resonance frequencies due to fabrication inaccuracies can be compensated by the index tuning, which is inherent in our schemes. In addition to optics, the underlying ideas and scheme are applicable to all wave phenomena, including acoustics and microwave signals.

## References


1. J. D. Joannopoulos, P. R. Villeneuve, and S. Fan, Photonic crystals: putting a new twist on light, *Nature* 386:143–149 (1997).
2. K. Vahala, Optical microcavities, *Nature* 424:839–846 (2003).
3. O. Painter, R. K. Lee, A. Scherer, A. Yariv, J. D. O'Brien, P. D. Dapkus, I. Kim, Two-dimensional photonic crystal defect laser, *Science* 284:1819–1821 (1999).
4. H. G. Park, S. H. Kim, S. H. Kwon, Y. G. Ju, J. K. Yang, J. H. Baek, S. B. Kim, Y. H. Lee, Electronically driven single-cell photonic crystal laser, *Science* 305:1444–1447 (2004).
5. M. Soljacic and J. D. Joannopoulos, Enhancement of non-linear effect using photonic crystals, *Nat. Mater.* 3:211 (2004).
6. M. F. Yanik, S. Fan, and M. Soljacic, High-contrast all-optical bistable switching in photonic crystal microcavities, *Appl. Phys. Lett.* 83:2739 (2003).
7. M. F. Yanik, S. Fan, M. Soljacic, and J. D. Joannopoulos, All-optical transistor action with bistable switching in a photonic crystal cross-waveguide geometry, *Opt. Lett.* 28:2506 (2003).
8. V. R. Almeida, C. A. Barrios, R. R. Panepucci, and M. Lipson, All-optical control of light on a silicon chip, *Nature* 431:1081–1084 (2004).
9. M. F. Yanik, H. Altug, J. Vuckovic, and S. Fan, Sub-micron all-optical digital memory and integration of nano-scale photonic devices without isolators, *IEEE J. Lightwave Tech.* 22:2316 (2004).
10. D. Psaltis, Coherent optical information systems, *Science* 298:1359–1363 (2002).
11. C. Liu, Z. Dutton, C. H. Behroozi, and L. V. Hau, Observation of coherent optical information storage in an atomic medium using halted light pulses, *Nature* 409:490–493 (2001).
12. D. F. Phillips, A. Fleischhauer, A. Mair, R. L. Walsworth, and M. D. Lukin, Storage of light in atomic vapor, *Phys. Rev. Lett.* 86:783 (2001).
13. E. J. Reed, M. Soljacic, and J. D. Joannopoulos, Color of shock waves in photonic crystals, *Phys. Rev. Lett.* 90:203904 (2003).
14. E. J. Reed, M. Soljacic, and J. D. Joannopoulos, Reversed Doppler effect in photonic crystals, *Phys. Rev. Lett.* 91:133901 (2003).
15. M. F. Yanik and S. Fan, Stopping light all-optically, *Phys. Rev. Lett.* 92:083901 (2004).
16. M. F. Yanik and S. Fan, Time reversal of light with linear optics and modulators, *Phys. Rev. Lett.* 93:173903 (2004).

17. M. F. Yanik, W. Suh, Z. Wang, and S. Fan, Stopping light in a waveguide with an all-optical analog of electromagnetically induced transparency, *Phys. Rev. Lett.* 93:233903 (2004).
18. M. F. Yanik and S. Fan, Stopping and storing light coherently, *Phys. Rev. A* 71:013803 (2005).
19. R. Ramaswami and K. N. Sivarajan, *Optical Networks: A Practical Perspective*, Morgan Kaufmann, San Francisco, CA, 1998.
20. M. D. Lukin and A. Imamoglu, Controlling photons using electromagnetically induced transparency, *Nature* 413:273 (2001).
21. L. M. Duan, M. D. Lukin, J. I. Cirac, and P. Zoller, Long-distance quantum communication with atomic ensembles and linear optics, *Nature* 414:413–418 (2001).
22. L. Brillouin, *Wave Propagation and Group Velocity*, Academic, New York, 1960.
23. K. J. Boller, A. Imamoglu, and S. E. Harris, Observation of electromagnetically induced transparency, *Phys. Rev. Lett.* 66:2593–2596 (1991).
24. A. Kasapi, M. Jain, G. Y. Yin, and S. E. Harris, Electromagnetically induced transparency: propagation dynamics, *Phys. Rev. Lett.* 74:2447–2450 (1995).
25. L. V. Hau, S. E. Harris, Z. Dutton, and C. H. Behroozi, Light speed reduction to 17 metres per second in an ultracold atomic gas, *Nature* 397:594–598 (1999).
26. M. M. Kash, V. A. Sautenkov, A. S. Zibrov, L. Hollberg, G. R. Welch, M. D. Lukin, Y. Rostovtsev, E. S. Fry, M. O. Scully, Ultraslow group velocity and enhanced nonlinear optical effects in a coherently driven hot atomic gas, *Phys. Rev. Lett.* 82:5229–5232 (1999).
27. D. Budker, D. F. Kimball, S. M. Rochester, and V. V. Yashchuk, Nonlinear magneto-optics and reduced group velocity of light in atomic vapor with slow ground state relaxation, *Phys. Rev. Lett.* 83:1767–1770 (1999).
28. A. V. Turukhin, V. S. Sudarshanam, M. S. Shahriar, J. A. Musser, B. S. Ham, P. R. Hemmer, Observation of ultraslow and stored light pulses in a solid, *Phys. Rev. Lett.* 88:023602 (2002).
29. M. S. Bigelow, N. N. Lepeshkin, and R. W. Boyd, Observation of ultraslow light propagation in a ruby crystal at room temperature, *Phys. Rev. Lett*. 90:113903 (2003).
30. Y. Yamamoto and R. E. Slusher, Optical processes in microcavities, *Phys. Today* 46:66–73 (1993).
31. E. Yablonovitch, Inhibited spontaneous emission in solid-state physics and electronics, *Phys. Rev. Lett.* 58:2059–2062 (1987).
32. S. John, Strong localization of photons in certain disordered dielectric superlattices, *Phys. Rev. Lett.* 58:2486–2489 (1987).
33. J. D. Joannopoulos, R. D. Meade, and J. N. Winn, *Photonic Crystals: Molding the Flow of Light*, Princeton, New Jersey, 1995.
34. D. K. Armani, T. J. Kippenberg, S. M. Spillane, and K. J. Vahala, Ultra-high-Q toroid microcavity on a chip, *Nature* 421:925–928 (2003).
35. M. Notomi, K. Yamada, A. Shinya, J. Takahashi, C. Takahashi, and I. Yokohama, Extremely large group velocity dispersion of line-defect waveguides in photonic crystal slabs, *Phys. Rev. Lett.* 87:253902 (2001).
36. N. Stefanou and A. Modinos, Impurity bands in photonic insulators, *Phys. Rev. B* 57:12127 (1998).
37. A. Yariv, Y. Xu, R. K. Lee, and A. Scherer, Coupled-resonator optical waveguide: a proposal and analysis, *Opt. Lett.* 24:711–713 (1999).
38. M. Bayindir, B. Temelkuran, and E. Ozbay, Tight-binding description of the coupled

defect modes in three-dimensional photonic crystals, *Phys. Rev. Lett.* 84:2140–2143 (2000).

39. G. Lenz, B. J. Eggleton, C. K. Madsen, and R. E. Slusher, Optical delay lines based on optical filters, *IEEE J. Quantum Electron.* 37:525–532 (2001).
40. A. Messiah, *Quantum Mechanics*, Interscience, New York, 1963.
41. S. Fan, P. R. Villeneuve, J. D. Joannopoulos, M. J. Khan, C. Manolatou, H. A. Haus, Theoretical analysis of channel drop tunneling processes, *Phys. Rev. B* 59:15882 (1999).
42. G. Juzeliunas and H. J. Carmichael, A systematic formulation of slow polaritons in atomic gases, *Phys. Rev. A* 65:021601R (2002).
43. A. Taflove and S. C. Hagness, *Computational Electrodynamics*, Artech House, Norwood, MA, 2000.
44. S. L. Chuang, *Physics of Optoelectronic Devices*, Interscience, New York, 1995.
45. Y. Xu, Y. Li, R. K. Lee, and A. Yariv, Scattering-theory analysis of waveguide-resonator coupling, *Phys. Rev. E* 62:7389–7404 (2000).
46. D. W. Vernooy, V. S. Ilchenko, H. Mabuchi, E. W. Streed, and H. J. Kimble, High-Q measurements of fused-silica microspheres in the near infrared, *Opt. Lett.* 23:247–249 (1998).
47. K. Vahala, *Optical Microcavities*, World Scientific, New Jersey, 2004.
48. M. Fink, Time-reversal of ultrasonic fields—Part I: basic principles, *IEEE Trans. Ultrason. Ferroelec. Freq. Contr.* 39:555–566 (1992).
49. I. Freund, Time-reversal symmetry and image reconstruction through multiple-scattering media, *J. Opt. Soc. Am. A* 9:456 (1992).
50. J. de Rosny and M. Fink, Overcoming the diffraction limit in wave physics using a time-reversal mirror and a novel acoustic sink, *Phys. Rev. Lett.* 89:124301 (2002).
51. G. S. Agarwal, A. T. Friberg, and E. Wolf, Scattering theory of distortion correction by phase conjugation, *J. Opt. Soc. Am.* 73:529–538 (1983).
52. A. Yariv, Three-dimensional pictorial transmission in fibers, *Appl. Phys. Lett.* 28:88 (1976).
53. R. A. Fisher, *Optical Phase Conjugation*, Academic, San Diego, 1984.
54. B. Y. Zel'dovich, N. F. Pilipetsky, and V. V. Shkunov, *Principles of Phase Conjugation*, Springer-Verlag, Berlin, 1985.
55. D. M. Marom, D. Panasenko, Sun Pang-Chen, Y. T. Mazurenko, and Y. Fainman, Real-time spatial-temporal signal processing with optical nonlinearities, *IEEE J. Quantum Elec.* 7:683 (2001).
56. D. M. Pepper, *Laser Handbook*, vol. 4, pp. 333, North-Holland Physics, Amsterdam, 1988.
57. V. Ilchenko, D. Kossakovski, I. Solomatine, D. Eliyahu, J. O'Brien, *Proceedings of the 28th Annual GOMACTech Conference*, Florida (2003).

Stanford University

(Received January 17, 2005)